Complex Media Microstrip Ridge Structures: Formulation and Basic Characteristics of Ferrite Structures

George W. Hanson, *Member, IEEE*

Abstract— Microstrip transmission lines residing on bianisotropic material ridges embedded in a multilayered environment are studied using a coupled set of integral equations (IE's). The full-wave IE formulation accounts for general linear media in the ridge region using equivalent polarization currents residing in a multilayered bianisotropic background. Numerical results showing basic propagation characteristics are presented for a variety of single and coupled ferrite ridge structures. It is shown that the use of finite width ferrite ridges as either substrates or superstrates can produce nonreciprocity while confining the ferrite material to a small area in the vicinity of the transmission line.

I. INTRODUCTION

PRINTED transmission lines embedded in nonreciprocal ferrite and magnetoplasma media allow for a variety of devices to be implemented in planar or quasiplanar form, including isolators, phase shifters, and circulators. Transmission line propagation characteristics can be controlled electronically by adjustment of the bias field, and mechanically by proper geometrical configuration.

In this paper, microstrip lines on material ridges are studied using a volume integral equation (IE) technique. The formulation is for general linear media, and numerical results are presented for the important special case of ferrite structures. It is shown that the use of ferrite ridges can provide some additional control over propagation characteristics. Ferrite ridge structures embedded in reciprocal media also can be used to achieve nonreciprocal action while limiting the ferrite material to the immediate vicinity of the device.

Previous work on transmission lines printed on finite width material ridges has utilized a variety of techniques. For shielded structures, several techniques have been used to analyze propagation characteristics. In [1], a combined integral equation/modal matching (IEMM) method was described, and a transition between a microstrip ridge and a dielectric waveguide was studied in [2]. A method of lines (MoL) analysis was presented in [3], [4], a mixed potential mode-matching method in [5], and a Green's impedance function approach in [6].

For open structures, a full-wave mixed spectral/space-domain IE method using wavelets was described in [7], and a quasistatic method was presented in [8]. The MoL with
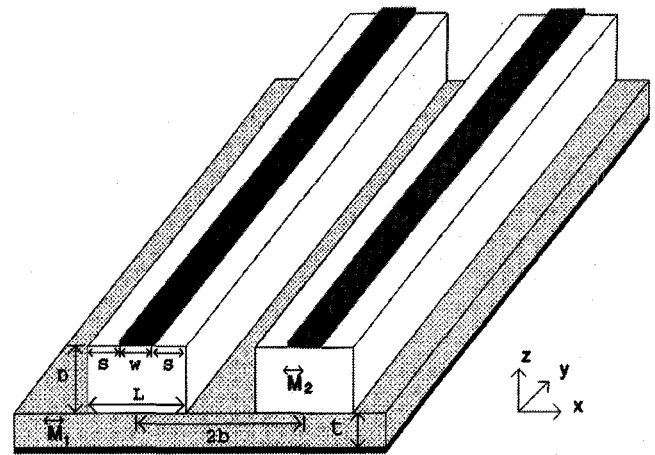
Fig. 1. Complex media microstrip ridge geometry.

a coordinate transformation (MoL/CT) [9], and MoL with absorbing boundary conditions (MoL/ABC) [10] were used to provide full-wave results. A special case of open microstrip ridge structure known as Microslab^{TM} was introduced in [11] for single structures, and coupled structures were examined in [12]. Other papers relevant to this work include modeling of dielectric waveguides using volume (or domain) IE techniques, [13]–[16] and references therein, among others. The volume IE method was originally developed for scattering problems [17], and has been used to analyze scattering from complicated material volumes.

The method described here is a generalization of the work presented in [18], where microstrip ridge structures with anisotropic permittivity embedded in isotropic media were considered. This method is also applicable to the study of single and coupled open bianisotropic waveguides by removing the conducting transmission lines. An $e^{j\omega t}$ dependance is assumed and suppressed throughout.

II. THEORY

The geometry of interest is shown in Fig. 1. Perfectly conducting, infinitely thin microstrip transmission lines and bianisotropic material ridge regions reside in the cover region of a layered media background environment. The constitutive parameters of the ridge regions and of the background environment can be expressed in 6 × 6 notation as

$$\overleftrightarrow{M} = \begin{bmatrix} \overleftrightarrow{\epsilon} & \overleftrightarrow{\mu} \\ \overleftrightarrow{\xi} & \overleftrightarrow{\zeta} \end{bmatrix}$$

where $\overleftrightarrow{\epsilon}$, $\overleftrightarrow{\mu}$, $\overleftrightarrow{\xi}$, $\overleftrightarrow{\zeta}$ are the permittivity, permeability, and optical activity dyadics, respectively. The four material dyadics are completely general, and the material in the ridge regions may be inhomogeneous in (x, z), while the infinite background substrate may be inhomogeneous along z. A coupled set of IE's can be formed by enforcing boundary conditions along the surface of the transmission lines and field conditions in the ridge regions. For simplicity, in the following development the multiple ridge regions are constructed from a single inhomogeneous region. The boundary and field conditions are given by

$$\hat{\alpha} \cdot \left\{ \sum_{n=1}^{N} \vec{e}_{\text{tn}}^{\,s}(x, D) + \vec{e}_{wg}^{\,s}(x, D) \right\} = -\hat{\alpha} \cdot \vec{e}^{\,\text{inc}}(x, D)$$
$$\dots \forall x \in W_m, \ m = 1 \dots N \quad (1a)$$

$$\vec{e}(x, z) - \sum_{n=1}^{N} \vec{e}_{\text{tn}}^{\,s}(x, z) - \vec{e}_{wg}^{\,s}(x, z) = \vec{e}^{\,\text{inc}}(x, z)$$
$$\dots \forall (x, z) \in S_{wg} \quad (1b)$$

$$\vec{h}(x, z) - \sum_{n=1}^{N} \vec{h}_{\text{tn}}^{\,s}(x, z) - \vec{h}_{wg}^{\,s}(x, z) = \vec{h}^{\,\text{inc}}(x, z)$$
$$\dots \forall (x, z) \in S_{wg} \quad (1c)$$

where W_m extends over the mth transmission line, S_{wg} denotes the space occupied by the ridge region, $\hat{\alpha} = (\hat{x}, \hat{y})$ are unit vectors tangential to the transmission lines, $\vec{e}_{\text{tn}}^{\,s}(\vec{h}_{\text{tn}}^{\,s})$ is the scattered electric (magnetic) field maintained by conduction current on the nth transmission line, $\vec{e}_{wg}^{\,s}(\vec{h}_{wg}^{\,s})$ is the scattered electric (magnetic) field due to equivalent polarization current in the inhomogeneous ridge region, $\vec{e}(\vec{h})$ is the total electric (magnetic) field in the ridge region, and $\vec{e}^{\,\text{inc}}(\vec{h}^{\,\text{inc}})$ is the incident electric (magnetic) field maintained by remote sources with the transmission lines and ridge region absent, but in the presence of the multilayered background environment. In the above, (1a) represents $2N$ scalar equations which force the total tangential electric field to be zero along the mth perfectly conducting transmission line. Equations (1b) and (1c), represent six scalar equations which force the total electric (magnetic) field at every point within the ridge region to equal the incident field plus the field maintained by the various currents. The radiation condition is enforced, along with boundary conditions at the other planar interfaces, by the Green's function for the background environment.

The formulation is carried out in the one–dimensional (1-D) spatial Fourier transform domain, with the transform pair $y \leftrightarrow k_y$. Since all material regions are linear, the electric and magnetic fields in the cover region are related to electric and magnetic currents by [19]

$$\vec{e}(\vec{\rho}, k_y) = \int_{S} \overleftrightarrow{G}^{\,e,e}(\vec{\rho} \mid \vec{\rho}\,', k_y) \cdot \vec{J}_e(\vec{\rho}\,', k_y) dS'$$
$$+ \int_{S} \overleftrightarrow{G}^{\,e,h}(\vec{\rho} \mid \vec{\rho}\,', k_y) \cdot \vec{J}_m(\vec{\rho}\,', k_y) dS'$$

$$\vec{h}(\vec{\rho}, k_y) = \int_{S} \overleftrightarrow{G}^{\,h,e}(\vec{\rho} \mid \vec{\rho}\,', k_y) \cdot \vec{J}_e(\vec{\rho}\,', k_y) dS'$$
$$+ \int_{S} \overleftrightarrow{G}^{\,h,h}(\vec{\rho} \mid \vec{\rho}\,', k_y) \cdot \vec{J}_m(\vec{\rho}\,', k_y) dS' \quad (2)$$

where $\vec{J}_{e(m)}$ is an electric (magnetic) current, $\overleftrightarrow{G}^{\,\alpha,\beta}$ is the dyadic Green's function which provides the vector field of type α due to a vector current of type β, and $\hat{\rho} = \hat{x}x + \hat{z}z$. In (2) the Green's functions are for the layered bianisotropic background environment, which are computed using the method presented in [20].

The volume equivalence principle is used to account for the inhomogeneous ridge region above the background layering [21]. The ridge region is replaced by a homogeneous region containing equivalent polarization currents which reside in the space previously occupied by the ridge and vanish outside of that region, as depicted in [18]. The equivalent currents for bianisotropic media can be derived from Maxwell's equations to yield [20]

$$\vec{J}_e^{\,\text{eq}}(x, z)$$
$$= j\omega[\overleftrightarrow{\epsilon}(x, z) - \epsilon_c \overleftrightarrow{I}] \cdot \vec{e}(x, z) + j\omega \overleftrightarrow{\xi}(x, z) \cdot \vec{h}(x, z)$$
$$\vec{J}_m^{\,\text{eq}}(x, z)$$
$$= j\omega[\overleftrightarrow{\mu}(x, z) - \mu_c \overleftrightarrow{I}] \cdot \vec{h}(x, z) + j\omega \overleftrightarrow{\zeta}(x, z) \cdot \vec{e}(x, z). \quad (3)$$

A coupled set of IE's is formed by substituting the relations (2) and (3) into the set of boundary and field conditions (1), resulting in

$$\hat{\alpha} \cdot \left\{ \sum_{n=1}^{N} \int_{x_n} \overleftrightarrow{G}^{\,e,e}(x, D \mid x', D) \cdot \vec{J}_{\text{tn}}(x', D) dx' \right.$$
$$+ j\omega \int_{S_{wg}} \overleftrightarrow{G}^{\,e,\text{eq}}(x, D \mid x', z') \cdot \vec{e}(x', z') dS'$$
$$\left. + \int_{S_{wg}} \overleftrightarrow{G}^{\,e,hq}(x, D \mid x', z') \cdot \vec{h}(x', z') dS' \right\}$$
$$= -\hat{\alpha} \cdot \vec{e}^{\,\text{inc}}(x, D) \quad \hat{\alpha} = \hat{x}, \hat{y}, \ \begin{matrix} x \in W_m \\ m = 1 \dots N \end{matrix} \quad (4)$$

from (1a)

$$\vec{e}(x, z) - \sum_{n=1}^{N} \int_{x} \overleftrightarrow{G}^{\,e,e}(x, z \mid x', D) \cdot \vec{J}_{\text{tn}}(x', D) dx'$$
$$- j\omega \int_{S_{wg}} \overleftrightarrow{G}^{\,e,\text{eq}}(x, z \mid x', z') \cdot \vec{e}(x', z') dS'$$
$$- \int_{S_{wg}} \overleftrightarrow{G}^{\,e,hq}(x, z \mid x', z') \cdot \vec{h}(x', z') dS'$$
$$= \vec{e}^{\,\text{inc}}(x, z) \quad \forall x, z \in S_{wg} \quad (5)$$

from (1b), and

$$\vec{h}(x, z) - \sum_{n=1}^{N} \int_{x} \overleftrightarrow{G}^{\,h,e}(x, D \mid x', D) \cdot \vec{J}_{\text{tn}}(x', D) dx'$$
$$- j\omega \int_{S_{wg}} \overleftrightarrow{G}^{\,h,hq}(x, z \mid x', z') \cdot \vec{h}(x', z') dS'$$
$$- \int_{S_{wg}} \overleftrightarrow{G}^{\,h,\text{eq}}(x, z \mid x', z') \cdot \vec{e}(x', z') dS'$$
$$= \vec{h}^{\,\text{inc}}(x, z) \quad \forall x, z \in S_{wg} \quad (6)$$

from (1c), where

$$\overset{\leftrightarrow}{G}{}^{e,\mathrm{eq}} = \overset{\leftrightarrow}{G}{}^{e,e} \cdot [\overset{\leftrightarrow}{\epsilon} - \epsilon_c \overset{\leftrightarrow}{I}] + \overset{\leftrightarrow}{G}{}^{e,h} \cdot \overset{\leftrightarrow}{\zeta}$$

$$\overset{\leftrightarrow}{G}{}^{e,\mathrm{hq}} = \overset{\leftrightarrow}{G}{}^{e,e} \cdot \overset{\leftrightarrow}{\xi} + \overset{\leftrightarrow}{G}{}^{e,h} \cdot [\overset{\leftrightarrow}{\mu} - \mu_c \overset{\leftrightarrow}{I}]$$

$$\overset{\leftrightarrow}{G}{}^{h,\mathrm{eq}} = \overset{\leftrightarrow}{G}{}^{h,h} \cdot \overset{\leftrightarrow}{\zeta} + \overset{\leftrightarrow}{G}{}^{h,e} \cdot [\overset{\leftrightarrow}{\epsilon} - \epsilon_c \overset{\leftrightarrow}{I}]$$

$$\overset{\leftrightarrow}{G}{}^{h,\mathrm{hq}} = \overset{\leftrightarrow}{G}{}^{h,h} \cdot [\overset{\leftrightarrow}{\mu} - \mu_c \overset{\leftrightarrow}{I}] + \overset{\leftrightarrow}{G}{}^{h,e} \cdot \overset{\leftrightarrow}{\xi} \, . \qquad (7)$$

The coupled set of IE's is solved using the method of moments (MoM). The conduction currents $(\vec{J}_{tn})$ on each transmission line are expanded in edge-weighted Chebyshev polynomials [18], [22]. The electric and magnetic fields in the ridge region are expanded as subdomain basis functions

$$\vec{e}(x,z) = \sum_{\beta=x,y,z} \sum_{n=1}^{N_e} \sum_{m=1}^{M_e} \hat{\beta} e^{\beta}_{n,m} P_n(x) R_m(z)$$

$$\vec{h}(x,z) = \sum_{\beta=x,y,z} \sum_{n=1}^{N_h} \sum_{m=1}^{M_h} \hat{\beta} h^{\beta}_{n,m} P_n(x) R_m(z)$$

$$(8)$$

where

$$P_n(x) = \begin{cases} \dfrac{\sin[k_e(h-|x-x_n|)]}{\sin(k_e h)} & |x - x_n| < h \\ 0 & \text{else} \end{cases} \qquad (9)$$

are overlapping piecewise sinusoidal (PWS) functions, with $R_m(z)$ having a similar definition. Half-PWS functions are used along the perimeter of the ridge regions in order to allow for nonvanishing fields there. The wavenumber parameter $k_e \approx 0.1 k_0$ causes the PWS functions to effectively model triangular functions, although results are generally insensitive to the value used. A Galerkin solution is implemented by testing each scaler IE with the appropriate function, leading to a matrix system. To determine propagation constants (k_y), the impressed field terms are set to zero and a numerical root search is performed to find the value of k_y which forces the determinate of the impedance matrix to vanish.

III. RESULTS

In order to verify the formulation and resulting numerical solution of the governing IE's, comparisons were made with isotropic microstrip ridge structures [10], [11]. The results agreed very well with those previously published, as shown in [18]. For ferrite structures, results for microstrip on a very wide ridge agreed with previously published values for microstrip lines embedded in infinite layered ferrite media [23], with less than 1% difference between values. Results for practical ridge structures should be considerably more accurate, since the region is electrically small and can be modeled with a modest number of PWS functions [18]. In order to verify the coupled ridge solution, several numerical tests were performed. The even mode became equal to the fundamental mode of the isolated double-width structure in the limit as the ridge spacing became small ($s = 0$), and tended toward the fundamental mode of the isolated ridge when the spacing became large, in agreement with known behavior. With the conducting strips removed, the even and
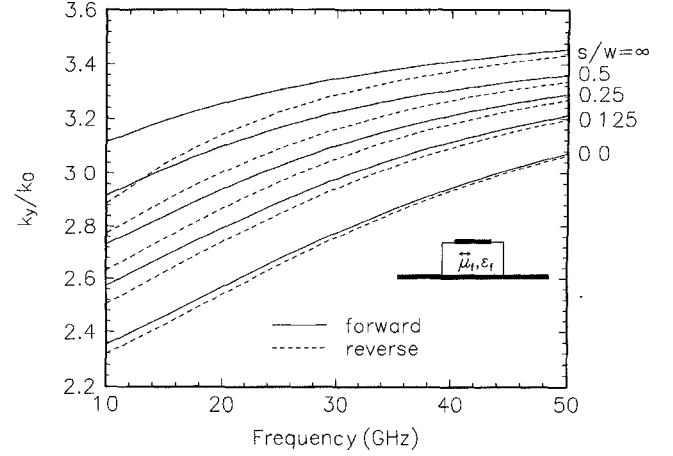

Fig. 2. Dispersion characteristics of a single microstrip ferrite ridge structure for various values of s/w, with $D = 0.1016$ cm, $t = 0$.

odd modes of the coupled ridge structure agreed with results presented in [14] for coupled strip dielectric waveguides.

In all of the following results the permittivity and permeability are relative to ϵ_0, μ_0, respectively, and the ferrite regions are described by isotropic permittivity ϵ_f and anisotropic permeability

$$[\mu_f] = R(\theta,\phi) \begin{bmatrix} \mu & j\kappa & 0 \\ -j\kappa & \mu & 0 \\ 0 & 0 & 1 \end{bmatrix} R^T(\theta,\phi)$$

where $\mu = 1 + (\omega_0 \omega_M)/(\omega_0^2 - \omega^2)$, $\kappa = (\omega \omega_M)/(\omega_0^2 - \omega^2)$, $\omega_0 = \gamma \mu_0 H_0, \omega_M = \gamma \mu_0 M_s$ and M_s is the material saturation magnetization, H_0 is the dc magnetic bias field, $\gamma = -1.759 \times 10^{11}$ kg/coul, and (θ, ϕ) are the angles of the applied magnetic field. Angles (θ, ϕ) are defined in the usual manner, with ϕ referenced to the x-axis with positive rotations toward the y-axis, and θ is referenced to the z-axis. The rotation matrices are

$$R(\theta,\phi) = \begin{bmatrix} \cos(\theta)\cos(\phi) & \cos(\theta)\sin(\phi) & -\sin(\theta) \\ -\sin(\phi) & \cos(\theta) & 0 \\ \sin(\theta)\cos(\phi) & \sin(\theta)\sin(\phi) & \cos(\theta) \end{bmatrix}$$

with R^T the transpose of R. For the results presented here, the ferrite material parameters are: $\epsilon_f = 12.6$, $\mu_0 M_s = 0.275$, $\phi = 0°$, $\theta = 90°$ (except for Fig. 3, where it varies), and $\omega_0 = 0.1 \omega_m$ (except for Fig. 4, where ω_0 varies with applied magnetic field). In all cases the transmission line has $w = 0.1016$ cm. Comments on convergence with regard to number of basis functions are included in [18], which generally apply to the formulation here.

In Fig. 2, dispersion characteristics are shown for a single microstrip ferrite ridge structure over a ground plane ($t = 0$), for various values of s/w, with $D = 0.1016$ cm. It can be seen that for $s/w = 0$, both forward and reverse waves are considerably faster than for $s/w = \infty$, due to the increased air region around the transmission line. Also, the differential phase shift (DPS), $k_y^+ - k_y^-$, is greatly reduced, since the field in the ferrite ridge region is mainly vertically oriented and does not fully sample the various ferrite permeability components.
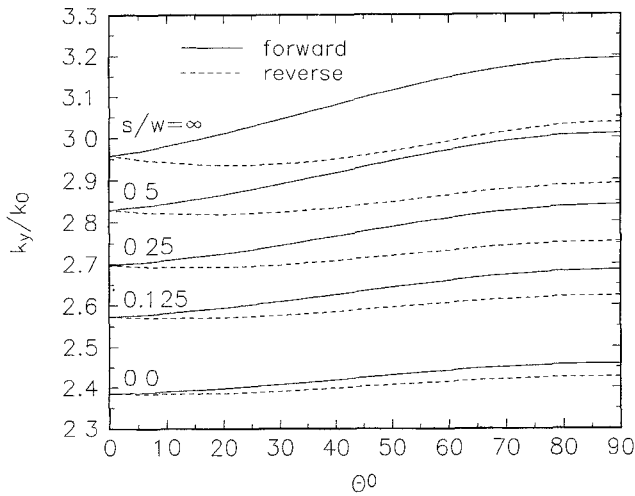
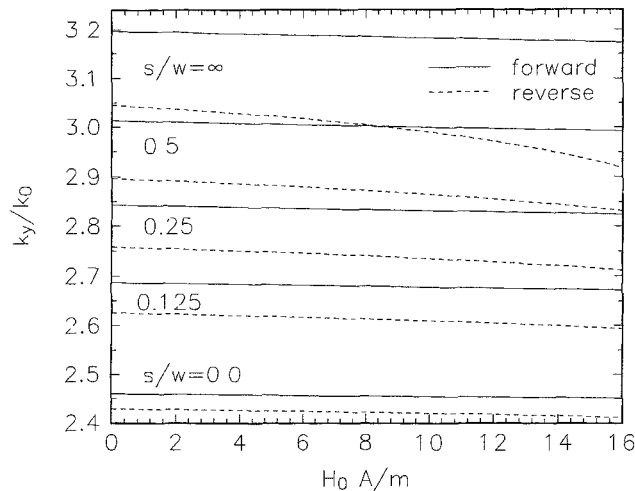Fig. 3.   Effect of varying the applied magnetic bias field angle θ on the structure considered in Fig. 2, at $f = 15$ GHz.
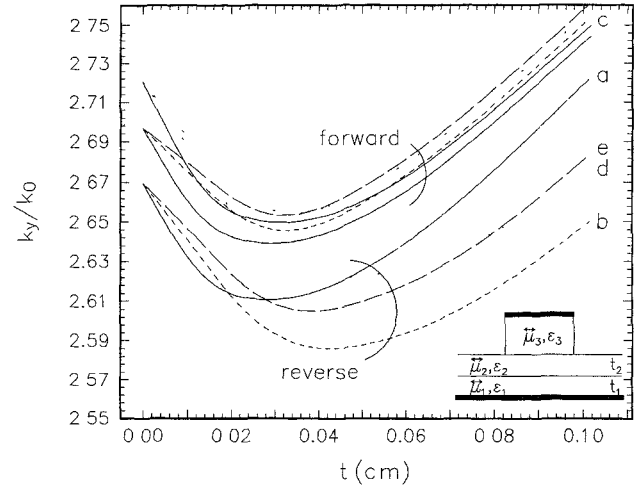

Fig. 5.   Propagation constant of a single microstrip ridge structure vs. substrate thickness $t_1 = t_2 = t/2$, with $D = 0.0508$ cm, $s/w = 0$, and $f = 15$ GHz. Five different cases are shown as explained in the text.

Fig. 4.   Effect of varying the applied magnetic bias field strength on the ridge structure considered in Fig. 2, with $f = 15$ GHz.

As s/w is increased, propagation behavior becomes similar to the $s/w = \infty$ case, which was generated using the method described in [20]. It should be noted that even a relatively small extension of the ridge region beyond the transmission line strip width results in DPS approaching the infinitely wide case.

The effect of varying the magnetic bias field angle is examined in Fig. 3, and of varying the applied magnetic field strength in Fig. 4, all for the ridge geometry depicted in the insert of Fig. 2 with $f = 15$ GHz. In both figures, propagation characteristics behave in a manner similar to that described for Fig. 2, where for $s/w = 0$ waves are considerable faster than for $s/w = \infty$, and DPS is reduced. A small extension of the ridge region beyond the transmission line width considerably affects the propagation constants.

In Fig. 5 the effect of adding an infinite substrate below the ridge region is examined, where propagation constant is shown as a function of substrate thickness t, with $D = 0.0508$ cm, $s/w = 0$, and $f = 15$ GHz. Five different cases are

considered:

a) ferrite ridge/isotropic substrate: $\vec{\mu}_3 = \vec{\mu}_f, \vec{\mu}_1 = \vec{\mu}_2 = \vec{I}$, $\epsilon_3 = \epsilon_f, \epsilon_1 = \epsilon_2 = 12.9$;

b) ferrite ridge/ferrite substrate: $\vec{\mu}_3 = \vec{\mu}_1 = \vec{\mu}_2 = \vec{\mu}_f$, $\epsilon_3 = \epsilon_1 = \epsilon_2 = \epsilon_f$;

c) isotropic ridge/isotropic substrate: $\vec{\mu}_3 = \vec{\mu}_1 = \vec{\mu}_2 = \vec{I}, \epsilon_3 = \epsilon_1 = \epsilon_2 = 12.9$

d) isotropic ridge/ferrite substrate: $\vec{\mu}_3 = \vec{I}$, $\epsilon_3 = 12.9$, $\vec{\mu}_1 = \vec{\mu}_2 = \vec{\mu}_f$, $\epsilon_1 = \epsilon_2 = \epsilon_f$;

e) ferrite ridge/ferrite+isotropic substrate: $\vec{\mu}_3 = \vec{\mu}_2 = \vec{\mu}_f$, $\vec{\mu}_1 = \vec{I}$, $\epsilon_3 = \epsilon_2 = \epsilon_f$, $\epsilon_1 = 12.9$;

where for all cases $t_1 = t_2 = t/2$. Other than for case c), where DPS $= 0$, it is seen that the largest DPS comes from case b) and the smallest from case a), as might be expected. Although not shown here, for $s/w > 0$ the DPS for case a), ferrite material only in the ridge region, was considerably larger than for $s/w = 0$, similar to the behavior observed in Figs. 2–4.

The effect of a ferrite ridge superstrate over a microstrip printed on an isotropic substrate was examined in Fig. 6, as a function of ridge width, for $D = 0.1016$ cm, $f = 15$ GHz, $t = 0.0508$ cm, and $\epsilon_1 = 12.9$. It can be seen that the forward and reverse waves have approximately the same propagation constant until the ridge width extends beyond the transmission line width ($w = 0.1016$ cm).

Coupled ridge structures are examined in Figs. 7 and 8, for two ferrite ridges. In Fig. 7 the two coupled ridge/microstrips are over a ground plane ($t = 0$), and in Fig. 8 the ridges reside on an isotropic substrate with $\epsilon_1 = 12.9$, $t = 0.0508$ cm. In both figures, $D = 0.0508$ cm, $L = 0.1016$ cm, $f = 15$ GHz, $s/w = 0$, and separation b varies. Both the forward and reverse waves split into even and odd modes, and converge toward the forward and reverse waves of the isolated ridge structure as the spacing is increased. It can be seen that when the ridges reside directly on the ground plane the two microstrips decoupled faster with increasing separation, compared to the ridge-on-substrate case.
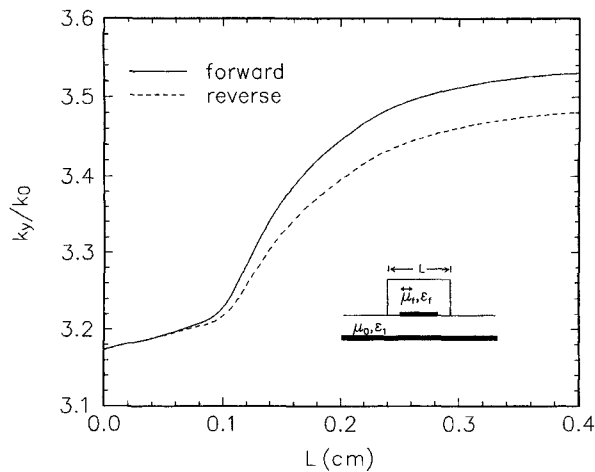
Fig. 6. Propagation constant of a structure comprised of a ferrite ridge superstrate over a microstrip printed on an isotropic substrate, as a function of ridge width L, $D = 0.1016$ cm, $f = 15$ GHz, $t = 0.0508$ cm, and $\epsilon_1 = 12.9$.
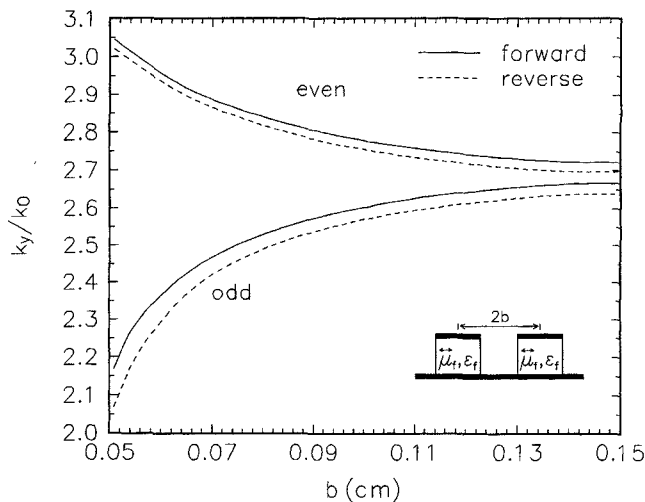

Fig. 7. Two coupled ferrite ridge structures over an infinite ground plane, $L = 0.1016$ cm, $D = 0.0508$ cm, $f = 15$ GHz, and $s/w = 0$.
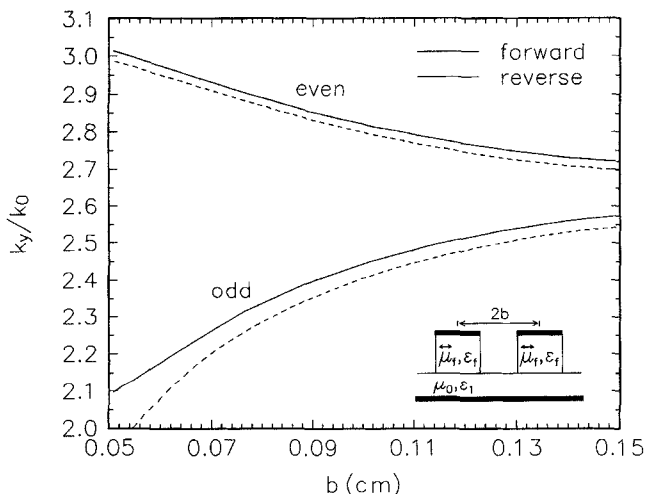

Fig. 8. Two coupled ferrite ridge structures over an isotropic substrate, $L = 0.1016$ cm, $D = 0.0508$ cm, $f = 15$ GHz, $t = 0.0508$ cm, $\epsilon_1 = 12.9$, and $s/w = 0$.

IV. CONCLUSION

Microstrip transmission lines residing on bianisotropic material ridges embedded in a multilayered environment have been studied using a coupled set of volume IE's. The full-wave IE formulation accounts for general linear media in the ridge region using equivalent polarization currents residing in a multilayered bianisotropic background. Numerical results have been presented showing basic propagation characteristics for the special case of ferrite ridges, which produce nonreciprocal action of varying extent depending on the ridge geometry and microstrip size and placement. Results for a variety of single and coupled ferrite microstrip ridge structures have been shown.

REFERENCES

[1] A. G. Engel and L. P. B. Katehi, "Frequency and time domain characterization of microstrip-ridge structures," *IEEE Trans. Microwave Theory Tech.*, vol. 41, pp. 1251–1261, Aug. 1993.

[2] A. G. Engel, N. I. Dib, and L. P. B. Katehi, "Characterization of a shielded transition to a dielectric waveguide," *IEEE Trans. Microwave Theory Tech.*, vol. 42, pp. 847–854, May 1994.

[3] M. Thorburn, A. Agoston, and V. K. Tripathi, "Computation of frequency-dependent propagation characteristics of microstriplike propagation structures with discontinuous layers," *IEEE Trans. Microwave Theory Tech.*, vol. 38, pp. 148–153, Feb. 1990.

[4] K. Wu and R. Vahldieck, "Comprehensive MoL analysis of a class of semiconductor-based transmission lines suitable for microwave and optoelectronic application," *Int. J. Numeric. Modeling*, vol. 4, pp. 45–62, 1991.

[5] C. C. Tzuang and J. Tseng, "A full-wave mixed potential mode-matching method for the analysis of planar or quasiplanar transmission lines," *IEEE Trans. Microwave Theory Tech.*, vol. 39, pp. 1701–1711, Oct. 1991.

[6] J. Huang and C. C. Tzuang, "Green's impedance function approach for propagation characteristics of generalized striplines and slotlines on nonlayered substrates," *IEEE Trans. Microwave Theory Tech.*, vol. 42, pp. 2317–2327, Dec. 1994.

[7] K. Sabetfakhri and L. P. B. Katehi, "Analysis of integrated millimeter-wave and submillimeter-wave waveguides using orthonormal wavelet expansions," *IEEE Trans. Microwave Theory Tech.*, vol. 42, pp. 2412–2422, Dec. 1994.

[8] C. E. Smith and R. S. Chang, "Microstrip transmission line with finite-width dielectric," *IEEE Trans. Microwave Theory Tech.*, vol. MTT-28, pp. 90–94, Feb. 1980.

[9] X. H. Yang and L. Shafai, "Full wave approach for the analysis of open planar waveguides with finite width dielectric layers and ground planes," *IEEE Trans. Microwave Theory Tech.*, vol. 42, pp. 142–149, Jan. 1994.

[10] A. Dreher and R. Pregla, "Analysis of microstrip structures with an inhomogeneous dielectric layer in an unbounded region," *IEE Electron. Lett.*, vol. 28, pp. 2133–2134, 1992.

[11] B. Young and T. Itoh, "Analysis and design of Microslab waveguide," *IEEE Trans. Microwave Theory Tech.*, vol. MTT-35, pp. 850–857, Sept. 1987.

[12] B. Young and T. Itoh, "Analysis of coupled Microslab^{TM} lines," *IEEE Trans. Microwave Theory Tech.*, vol. 36, pp. 616–619, Mar. 1988.

[13] J. S. Bagby, D. P. Nyquist, and B. C. Drachman, "Integral equation formulation for analysis of integrated dielectric waveguides," *IEEE Trans. Microwave Theory Tech.*, vol. MTT-33, pp. 906–915, Feb. 1987.

[14] J. Kiang, S. M. Ali, and J. A. Kong, "Integral equation solution to the guidance and leakage properties of coupled dielectric strip waveguides," *IEEE Trans. Microwave Theory Tech.*, vol. 38, pp. 193–203, Feb. 1990.

[15] H. P. Urbach and E. Lepelaars, "On the domain integral equation method for anisotropic inhomogeneous waveguides," *IEEE Trans. Microwave Theory Tech.*, vol. 42, pp. 118–126, Jan. 1994.

[16] H. J. M. Bastiaansen, N. H. G. Baken, and H. Blok, "Domain-integral analysis of channel waveguides in anisotropic multi-layered media," *IEEE Trans. Microwave Theory Tech.*, vol. 40, pp. 1918–1926, Oct. 1992.

[17] J. H. Richmond, "Scattering by a dielectric cylinder of arbitrary cross section shape," *IEEE Trans. Antennas Propagat.*, vol. AP-13, pp. 334–341, Mar. 1965.

[18] G. W. Hanson, "Propagation characteristics of microstrip transmission lines on anisotropic material ridges," *IEEE Trans. Microwave Theory Tech.*, vol. 43, pp. 2608–2613, Nov. 1995.

[19] C. H. Papas, *Theory of Electromagnetic Wave Propagation*. New York: McGraw-Hill, 1965.

[20] G. W. Hanson, "A numerical formulation of Dyadic Green's functions for planar bianisotropic media with application to printed transmission lines," *IEEE Trans. Microwave Theory Tech.*, Jan. 1996.

[21] R. F. Harrington, *Time-Harmonic Electromagnetic Fields*. New York: McGraw-Hill, 1961.

[22] J. S. Bagby, C. Lee, Y. Yuan, and D. P. Nyquist, "Entire-domain basis MoM analysis of coupled microstrip transmission lines," *IEEE Trans. Microwave Theory Tech.*, vol. 40, pp. 49–57, Jan. 1992.

[23] F. Mesa, R. Marques, and M. Horno, "An efficient numerical spectral domain method to analyze a large class of nonreciprocal planar transmission lines," *IEEE Trans. Microwave Theory Tech.*, vol. 40, pp. 1630–1640, Aug. 1992.

George W. Hanson, photograph and biography not available at the time of publication.